Optics for a volume holographic grating spectrograph for the Southern Astrophysical Research (SOAR) Telescope

Clemens, J. Christopher, Epps, Harland, Seagroves, Scott

J. Christopher Clemens, Harland W. Epps, Scott Seagroves, "Optics for a volume holographic grating spectrograph for the Southern Astrophysical Research (SOAR) Telescope," Proc. SPIE 4008, Optical and IR Telescope Instrumentation and Detectors, (16 August 2000); doi: 10.1117/12.395469

SPIE.

Event: Astronomical Telescopes and Instrumentation, 2000, Munich, Germany

Optics for a Volume Holographic Grating Spectrograph for the Southern Astrophysical Research (SOAR) Telescope

J. Christopher Clemens[a], Harland W. Epps[b], and Scott Seagroves[b]

[a]University of North Carolina, Department of Physics and Astronomy, CB3255, Chapel Hill, NC 27599
[b]UCO/Lick Observatory, Santa Cruz, CA 95046

ABSTRACT

We describe a novel optical design for a low-resolution imaging spectrograph that incorporates volume phase holographic (VPH) gratings. This spectrograph will provide imaging over a 5' square field of view, and single or multi-object spectroscopy with resolutions between 1000 and 8000. Our design choices have been dominated by a desire to preserve the superb image quality the SOAR telescope is expected to deliver, and to maximize throughput over the wavelength range of 320 to 850 nm. The resulting design is unusual in two respects: the angle between the collimated beam and camera optical axis is mechanically variable to exploit the efficiency advantages of volume holographic gratings, and all the optical elements are refracting, to maintain high throughput in the ultraviolet. In addition to the pre-construction collimator and camera designs for the spectrograph, we also present our evaluation of sample volume phase holographic gratings to illustrate the advantages and difficulties they present for astronomical spectroscopy.

Keywords: astronomical spectrograph, volume holographic grating, ultraviolet

1. A SPECTROGRAPH FOR THE SOAR TELESCOPE

The Southern Astrophysical Research (SOAR) Telescope is a 4.25 m f/16 telescope currently under construction on Cerro Pachon, Chile[1]. Its most distinctive feature will be superb image quality over a small field (around 8' diameter), obtained through a combination of excellent intrinsic seeing at the Cerro Pachon site (median 0.5" at 550 nm) and low order adaptive optics correction (tip-tilt). The telescope has been specified to degrade seeing by no more than 0.18" and individual instruments may add no more than 0.18" additional degradation. The SOAR partners have prepared a document describing in detail how the SOAR telescope and its initial instrument complement will capitalize on the advantage provided by superior image quality[2].

The spectrograph we describe in this paper will reside at one of the two SOAR Nasmyth foci, and will fulfil the SOAR partners' need for high throughput optical imaging and low-resolution spectroscopy. At the request of the donors who have provided major funding for its construction, it is called the Abraham Goodman Spectrograph. Besides meeting the image quality requirements stipulated by SOAR, our main design goal for the Goodman spectrograph has been to maximize throughput from the atmospheric cutoff near 320 nm to the Ca II triplet near 850 nm. This has led us to investigate volume phase holographic (VPH) gratings as described by Barden et al.[3], because of their potential advantages in efficiency compared to surface relief gratings.

Unfortunately, the properties of VPH gratings relevant to their use in astronomical applications are not well known, in spite of a large quantity of literature describing their features[4]. Consequently, before beginning an expensive and elaborate design, we embarked on a program to evaluate samples of VPH gratings. In the next section we summarize some of our measurements and conclude that the advantages offered by VPH gratings justify the development effort and expense required to build a spectrograph incorporating them. In the final section, we present a detailed optical design study by Harland Epps. The camera and collimator described there meet or exceed our original goals in every respect, and when constructed will become the heart of an extremely high-performance spectrograph.

In *Optical and IR Telescope Instrumentation and Detectors*, Masanori Iye, Alan F. M. Moorwood, Editors, Proceedings of SPIE Vol. 4008 (2000) • 0277-786X/00/$15.00

2. VOLUME PHASE HOLOGRAPHIC GRATINGS

VPH gratings disperse light via Bragg diffraction within a volume of material whose optical density or refractive index is modulated. Barden et al.[3] evaluated a VPH grating made by Kaiser Optical Systems, Inc. (KOSI) that exhibited higher peak efficiency at 700 nm than a comparable ruled, blazed grating in use at NOAO. More importantly, by changing the grating tilt to satisfy the Bragg condition for different wavelengths, Barden et al. found they could tune the efficiency maximum to values between 400 to 800 nm, and perhaps beyond, while maintaining a peak efficiency near 80%. This tunability represents one of the principal advantages of VPH gratings, because it insures that efficiency maximum will always lie at the wavelength of primary interest. This can often result in gains well above those implied by direct comparison of peak efficiencies. Furthermore, because VPH gratings are usually transmission gratings, they avoid the UV losses incurred in reflections from most materials, including reflection gratings, and they make it easy to implement an imaging mode.

The main disadvantage to using VPH gratings is the increased mechanical complexity required to use them effectively, mainly in the form of a changeable camera collimator angle. Also, as we discuss below, in the limit of short wavelength and large fringe spacing, it becomes difficult to construct VPH gratings that match the efficiency of blazed surface relief gratings. Finally, our ignorance of many of the properties of VPH gratings and our inexperience at writing realistic specifications for grating manufacturers is a drawback of VPH gratings we hope to improve with ongoing studies like that presented in this section.

2.1 Theory

The theoretical properties of volume holographic gratings have been explored in a large number of papers. We recommend the review by Gaylord & Moharam[4] for a summary. In this report we focus on the minimum theory necessary to understand basic grating properties. These rudiments provide a valuable guide for specifying grating properties to manufacturers, and for estimating limits to grating performance. We will use them in section 2 to motivate our empirical investigations of sample gratings.

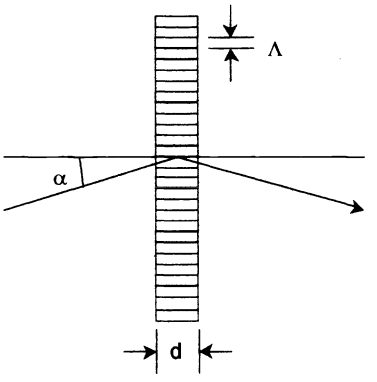

Figure 1: Geometry of a grating with fringes parallel to the surface normal. The glass substrate has been omitted from this idealization.

We will restrict our discussion to the case where fringe planes are parallel to the surface normal of the grating (Figure 1). This restriction is not a practical necessity, but offers several advantages. The incident and emergent beams will have approximately the same angle with the surface normal, which means the same anti-reflection coating, presumably tuned to a mean of the working angles, can be used on both external surfaces of the grating. Second, the largest number of transmitted diffraction orders emerge from the glass in this condition. Barden et al.[3] showed that higher diffraction orders can have useful efficiency when the angle of the grating is increased until it satisfies the appropriate Bragg condition. Finally, the construction of these gratings is simpler and more reliable, because slanted fringes tend to curve in the processing required to create refractive index modulations in the exposed emulsion[5].

Under the restricted geometry pictured in Figure 1, the Bragg condition is

$$m\lambda = \Lambda 2n\sin(\alpha), \qquad (1)$$

where m is the integer order, λ is the wavelength, Λ is the grating period, n is the refractive index of air, and α is the incident angle. Equation 1 is a condition for efficient diffraction at specified wavelength, but it is not sufficient for understanding grating efficiency. Precisely modeling grating efficiency requires solving a set of coupled second order linear differential wave equations. These equations describe wave propagation for all relevant reflected and transmitted diffraction orders (see Gaylord and Moharam[4]).

The approximate theory of Kolgelnik[6] is extremely useful for developing intuition about how gratings with different parameters behave. Kogelnik derived closed solutions to the wave equations retaining only the 0th and 1st transmitted orders. His formulae yield sinusoidally modulated efficiencies with maxima of 100% in a single order. The Kolgelnik approximation is generally valid when

$$\rho \equiv \frac{\lambda^2}{\Lambda^2 n_2 \Delta n_2} \geq 10, \qquad (2)$$

where Δn_2 is the amplitude of the modulations in the refractive index of the diffracting medium (n_2). This condition is a composite criterion that usually keeps the efficiency losses due to the propagation of unwanted orders to less than 1%[7].

For the Goodman spectrograph, we want gratings that are highly efficient, meaning that they diffract most incident light into a single order when operating near the Bragg condition for that order. This is the same condition that makes the Kolgelnik approximation valid, so we may think of equation 2 as a prescription for making highly efficient gratings. Gratings built to satisfy equation 2 operate in the "Bragg regime", where almost all of the incident power is transmitted into a single order. For our purposes, the grating period, Λ, and the wavelength, λ, will be dictated by the design parameters of the spectrograph, and n_2 by the emulsion properties, leaving Δn_2 as the only adjustable parameter.

Equation 2 provides a necessary but not sufficient condition for high efficiency gratings. Using Kolgelnik's approximations, the efficiency at Bragg angle for a selected wavelength is given by

$$\eta = \sin^2\left[\frac{\pi \Delta n_2 d}{\lambda \cos(\alpha_{2B})}\right]. \qquad (3)$$

The subscript 2 indicates that α now refers to the Bragg angle within the grating medium. The B is a reminder that this formula is only valid at the Bragg condition, i.e. the values used for λ and α in this equation must satisfy equation 1 within the medium. As a consequence, equation 3 is not appropriate for calculating efficiency envelopes at a single angle, rather, it shows how the efficiency maximum drops as the grating angle is "tuned" to different Bragg angles.

The Bragg efficiency given by formula 3 reaches 100% when the argument of the sin function is a multiple of $\pi/2$. Physically, d is the grating thickness and $d/\cos(\alpha)$ is the projected thickness for transmitted light, so we can think of $\Delta n_2 d/\cos(\alpha)$ as a projected "effective thickness" of the grating. The efficiency reaches a maximum when this "effective thickness" is equal to a half integer number of wavelengths. Here again, the wavelength and Bragg angle will be determined by scientific requirements, leaving Δn_2 and the grating thickness d as free parameters for optimizing the efficiency at a chosen wavelength.

In addition to completing the prescription for making highly efficient gratings at a single wavelength, equation 3 also provides a way to estimate how "tunable" a grating will be. Barden et al.[3] found that the peak efficiency of the 600 l/mm KOSI grating they tested could be moved from 400 to 800 nm by changing the angle from 8 to 14 degrees, without much drop in peak efficiency. Formula 3 suggests that a 600 l/mm grating built to operate in the Bragg regime would not be as versatile. A grating optimized for 700 nm operation using equation 3 would have very low efficiency when tuned to the Bragg condition near ½ that wavelength ($\cos(\alpha_{2B})$ is changing so slowly that at 350 nm η is approximately $\sin^2(\pi)=0$). Based on the high efficiency at 400 nm, Barden's grating showed better tunability but lower peak efficiency at design wavelength (700 nm) than expected from a Bragg regime grating, suggesting that there is a design trade between these 2 quantities. We will return to this trade in the next section.

As a final complication, equations 2 and 3 are appropriate for light polarized perpendicular to the plane of incidence, but must be reduced by a term that depends on incident angle for the opposite polarization state. At Bragg angles near 45 degrees this will reduce efficiency and polarize the ouput light. We can minimize these problems by restricting the Bragg angle to less than ~30 degrees within the diffracting medium.

2.2 Practice

In practice, specifying a grating reduces from a complex modeling problem to chosing the two parameters d and Δn_2 for a set of gratings with different Λs covering the range of resolutions we want (or can realistically achieve) in our spectrograph. In dichromated gelatin (DCG), the most common material for VPH elements, there are limits to the values Δn_2 and d can assume. KOSI typically uses thicknesses between 4 and 20 μm, with Δn_2 up to 0.10. Ralcon Development Labs provides a useful discussion of these parameters on their web page[8], giving 25 μm and 0.25 as practical upper limits for DCG.

Applying these constraints, and using 1.35 as the average refractive index of DCG, we find that for short wavelengths (e.g. 350 nm), it is not possible to satisfy equations 2 and 3 simultaneously for grating frequencies lower than 600 l/mm. In this limit, equation 2 requires Δn_2 to be so small that no practical value for d in equation 3 can compensate. This is not as terrible a situation as it may seem at first: equation 2 is the condition required for the Kolgelnik formulae to apply within 1%. Useable gratings can be made with lower values of ρ, but the theoretical efficiency will be <99%. Also, because of the λ_2 dependence of ρ, low frequency gratings (< 600 l/mm) will generally exhibit lower efficiency in the UV than at optical wavelengths. The measurements we describe in the next section show the results of this effect.

Predictions for gratings not designed for Bragg regime operation cannot be made without rigorous coupled wave analysis, but our limited experience shows that the "as constructed" properties do not match these detailed models. Consequently, we have spent our efforts on measurements rather than theoretical modeling. We have acquired and tested 7 different examples of VPH gratings. Four of these were samples provided at no charge by Dr. Richard Rallison of Ralcon Development Laboratories. Two were purchased under contract from the same lab, and the final one was built by Kaiser Optical Systems, Inc. There is not space in this paper to present all our results, so we will focus on those most relevant for the Goodman Spectrograph.

2.3 Measurements

We began our tests with UV efficiency measurements of a 1990 l/mm sample grating from Ralcon, because it was the first grating we acquired optimized for operation in the UV (355nm). UV efficiency is the main concern for our spectrograph not addressed by the measurements of Barden et al.[3] This sample has a DCG emulsion about 5 um thick and with refractive index modulation of about 0.1 in amplitude. These parameters were apparently chosen to optimize efficiency at various wavelengths on the basis of equation 3; we are not aware that they were the subject of any rigorous coupled wave analysis. The fringe planes in this grating are tilted so that the Bragg condition for 355 nm light is met when the incident angle is parallel to the surface normal.

The light source we used for evaluation consisted of a feedback-stabilized 100 W quartz-tungsten-halogen lamp coupled to an integrating sphere. We fed light from the integrating sphere into an Oriel monochromater with matched entrance and exit slits chosen to yield a 2 nm bandpass. Light from the output slit was collimated using a 3" diameter fused silica singlet, and then passed through a 3" variable iris, which we adjusted to reduce the beam size so that it fit within the active area of the grating. We mounted the grating on a rotation stage behind the iris, and could remove it from the beam without disturbing any of the optics. Finally, we re-imaged the slit onto our detector using another singlet with ½ the focal length of the collimator. Our detector was a Pixelvision spectroscopic camera with a UV-AR coated, thinned, back-illuminated SITe CCD. It was thermoelectrically cooled to reduce the dark count below 1 electron /s for the short integrations we required.

To measure the absolute efficiency of the grating, we took separate images of the slit with the grating in and out of the beam for a range of wavelengths at each grating angle. For each slit image we also acquired a background image by occulting the light at the exit slit. We subtracted these from the slit images to remove the bias and stray light. We did not apply a flat field correction, because tests showed that the slit image varied by less than 1% with position on the CCD. The ratio of the counts in the diffracted image of the slit to those in the direct image is the measured diffraction efficiency of the grating. The combined errors from all identified sources yield 1 σ error bars typically less than 1%. To reduce the possibility of systematic

errors, we repeated a subset of the measurements on 4 separate days, after disassembling and reassembling portions of the test equipment. Our results were consistent within the error bars.

Figure 2 shows efficiency measurements in the UV for the Ralcon 1990 l/mm grating, and answers the question of whether volume holographic gratings can operate efficiently in the UV. The measured efficiency is almost 75 % at 370. This is especially remarkable considering that the glass substrate of the grating is low iron glass with significant UV absorption. To understand how absorption affects the efficiency, and how it might improve if a similar grating were constructed on fused silica, we measured transmission losses by narrowing our collimated beam and passing it through a section near the edge of the grating that did not include the hologram. These measurements are the upper line in the figure.

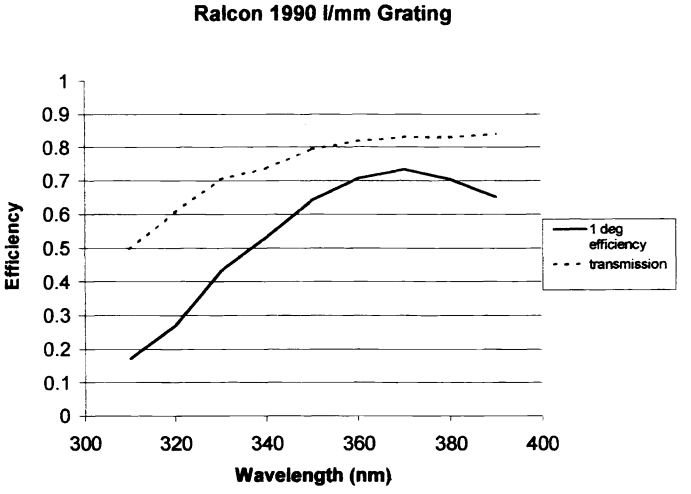

Figure 2: Absolute efficiency for the 1990 grating at 1degree incidence. The upper line shows the transmission of the glass.

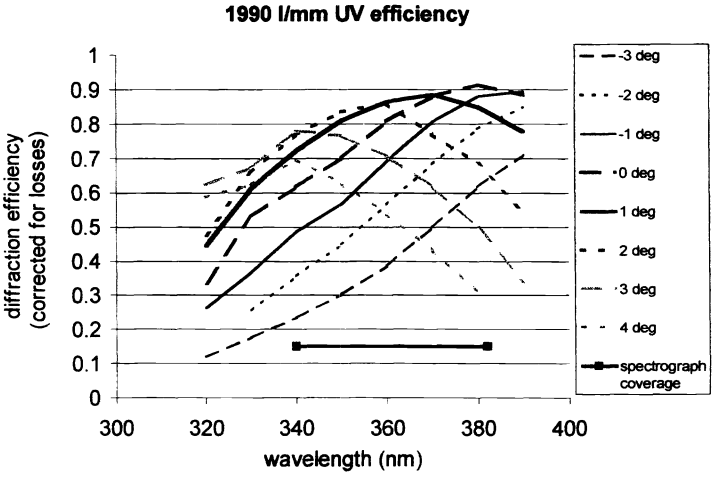

Figure 3: Diffraction efficiencies at various angles, corrected for transmission losses. The black bar shows the size of the spectral region our spectrograph will cover.

To test for tunability in the UV we measured efficiencies at different incident angles. Figure 3 shows the results. As Barden et al. found, the efficiency envelope moves with incident angle. The efficiencies in this plot have been corrected for the transmission and reflection losses to estimate the true diffraction efficiencies. With careful choices for material and coating, we should be able to achieve curves within 5%-10% of those shown. If so, we will have the most efficient UV grating ever used for astronomical research.

We also evaluated a sample grating with 474 l/mm fringe spacing. Because it was not designed for use in the UV and was made with UV absorbing adhesive, we are not confident of the reliability of our short wavelength measurements. However, we wanted to see if this grating showed properties similar to the one evaluated by Barden[3]. Figure 4 shows the results of measurements at three different incident angles. The peak efficiency is 75%, but with the addition of anti-reflection coatings and better glass substrate this grating would be over 80% efficiency at optical wavelengths, superior to the figures Barden et al. measured for their 600 l/mm grating.

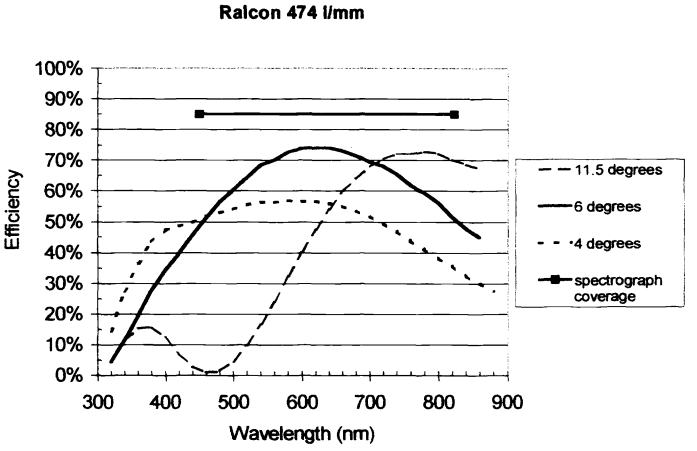

Figure 4: Absolute efficiencies for the 474 l/mm grating, uncorrected for transmission and reflection losses.

Subsequent to our measurements of the sample gratings, we received a custom 600 l/mm grating from KOSI. This was the product of an attempt to make a grating that could be tuned for efficient use over our entire wavelength range. The result is a highly tunable grating with disappointing efficiency; the maximum nowhere exceeds about 70%. This grating was the first we acquired with the correct dimensions for our spectrograph and with a substrate of AR coated fused silica. Unfortunately measurements using an optical flat show that the grating is curved into a concave cylinder on each side, with a peak to valley deviation of more than 1 μm. Detailed measurements of this grating, including a comparison to the preconstruction models, will be the subject of a future paper. Based on the outcome of this experiment, we have altered our specification strategy. Because it appears that the gratings produced have lower efficiency but higher bandwidth than the models, future gratings will be specified to maximize efficiency, the more difficult model parameter to achieve in production.

Finally, just before this article was submitted, we received the results of an attempt by Ralcon Development labs to produce our most difficult grating, the 300 l/mm. Quick tests of the maximum efficiency show that it is only about 50%, consistent with our expectation from equations 2 and 3 that low density, high efficiency gratings will be hard to produce using the thickest 25μm emulsion. We are currently discussing with Ralcon the possibility of stacking 2 layers of emulsion to give greater thickness, but it is possible that using a grism will be a better strategy for the lowest resolutions. The good news is that by using the slower curing Epotek 301-2 epoxy on the Ralcon grating and allowing it to cure at room temperature over 2 days, the final product remains flat to better than 0.4 λ, which was the original substrate flatness. We will publish evaluations of this grating after we have had a chance to measure it more thoroughly.

3. OPTICS FOR THE GOODMAN SPECTROGRAPH

In this section, we present the results of a study whose purpose was to identify and to develop an optical design plan for the Goodman spectrograph. In particular, we present suggested preconstruction optical designs for the essential collimator and camera and then analyze them to evaluate the desired performance characteristics. The optical designs are given in this report in full quantitative detail to enable others to analyze them and to comment on them also. The following parameters, requirements and optical design goals were used to guide the design study:

1. The spectrograph must have good response from the atmospheric cutoff through the visible and into the very near infrared. It is *required* to reach from 320 to 850 nm with excellent image quality and throughput.

2. The spectrograph optics should be *all-refracting* so as to avoid the use of mirrors. Refractive materials should be limited to fused silica and synthetically-grown optical crystals such as CaF2, BaF2, LiF, NaCl, etc., which have essentially 100% internal transmission throughout the spectral range of interest. Optical glass *should not be used* for the refracting optics as that would compromise the spectrograph's photon efficiency, especially in the UV. The choice of a coupling medium for contacted lens surfaces should also be made with good UV transmission as a primary concern.

3. It is a design goal to re-image a 5.0' x 5.0' field at the telescope focus upon a flat , 2048 x 2048 x 15-μm CCD area at the camera focus.

4. It is a design goal that *system* image quality in imaging mode (including degradation by collimator and camera residual aberrations as well as sampling limitations due to the CCD's finite pixel size) shall be such that the point-spread-functions (PSF's) shall not degrade a 0.50-arcsec image diameter by more than 0.18 arcsec. Image diameter is defined here as the full-width-at-half-maximum (FWHM). Clearly, *outstanding image quality* is a primary optical design driver.

5. Dispersion will be provided by VPH transmission gratings with 300, 600, 900, 1200 lines/mm and possibly finer spacings up to 2400 lines/mm. The included angle Q (between collimated beam and camera optic axis) will be *mechanically variable* from 0.0 to 90.0 degrees. Q will be chosen to satisfy the VPH grating-blaze condition for any central wavelength of interest. If the VPH fringes are normal to the grating surface (as usually chosen), the grating angle will be Q/2 such that in effect, the symmetry implies Littrow operation for the central wavelength.

6. The spectrograph will be used at low dispersion some of the time such that a large fraction of the passband will be covered in a single exposure. It would be useful therefore for the collimator and the camera to be able to accommodate the entire 320-850 nm passband *without refocus* in spectroscopic mode if that is practical.

7. It is a design goal to provide a maximum spectral resolution of about 8000 at a wavelength of 500 nm and with a 0.50-arcsec slit width). Resolution is defined here in a 3-pixel-sampling sense.

8. The spectrograph's beam diameter should not exceed 75.0 mm in this initial study. This limit is imposed largely to avoid excessive "in-line" optical path-lengths in the design.

9. The total length along the optical axis from the telescope focal surface to the vertex of the last collimator element *plus* the length from the first camera element vertex to the camera focal plane shall not exceed 1641 mm. This requirement *assumes* that both of the referenced elements are lenses and that the referenced surfaces are both convex. This limit is imposed largely by the anticipated maximum length capacity of SOAR's Nasmyth platform(s).

10. The collimator's exit pupil distance should be at least 137.5 mm and the camera's entrance pupil distance should be at least 87.5 mm so as to provide space between the collimator and the grating for optical filters and to avoid any potential mechanical collision as the VPH grating is rotated to effect the blaze condition described in item 5. If the sum of these lengths exceeds 225.0 mm, then the excess length must be subtracted from the 1641-mm constraint described in item 9 so that a total length constraint of 1866 mm is conserved.

11. The spectrograph will be used in a long-slit mode and in a direct-coupled multi-slit mode. In the multi-slit mode, slitlets will be aligned perpendicular to dispersion and placed anywhere within the 5.0' x 5.0' imaging-field area but in such a way that the individual spectra do not overlap.

12. The detector will be (at least) a 2048 x 4096 x 15μm CCD with the dispersion running in the long direction. The camera f.o.v. must service the 68.7-mm diagonal so as to be able to cover the detector to its corners with sharply focused spectra. For reasons having to do with CCD functional details, it may be more advantageous to use a 4096 x 4096 x 15μmCCD. If so, it may become desirable to increase the collimator's and/or the camera's f.o.v. in a later study if it appears that could be done with minor changes to the baseline design.

13. The camera should have its back focal distance (b.f.d.) chosen such that no part of the final optical element (vacuum dewar lens) will be closer than 8.0 mm to the CCD surface. This constraint is intended to reduce unwanted potential ghost images by back-reflection off of the CCD to an acceptably low light level.

14. It is assumed that high-efficiency antireflection (AR) coatings will be used on all exposed optical surfaces. Nonetheless, attention should be paid to minimizing the number of exposed surfaces to avoid light loss and to avoid potential ghost images and/or ghost pupils by back reflection (off of the CCD in particular).

15. Where possible, the individual curvatures of the elements should be chosen so as to mitigate against refocusing of back reflected ghost images and/or ghost pupils upon the CCD.

3.1 Instrument Parameters Implied by Stipulated Conditions

The advantages of using as large a collimated beam as is feasible in a spectrograph are well known. Adopting the 75.0 mm maximum beam diameter given in item 8 and matching to the telescope's f/16.0 cone, one derives a 1200.0 mm focal length for the collimator. The telescope scale implies a 138.2 mm diagonal dimension across the imaging-field area mentioned in item 3. Therefore the collimator field radius must be at least 3.30 degrees to support the direct-imaging requirement.

The 4.25 m f/16.0 telescope will have a focal length of 67.20 m which yields an imaging scale of 325.8 μm/arcsec. The reimaging requirement mentioned in item 3 implies demagnification by a factor of 3.1816 which must therefore become the ratio of the collimator focal length to that of the camera (assuming that parallel light is passed between them to the grating). Thus one derives a 377.2 mm focal length for the camera. The reimaged scale will be 6.827 pixels/arcsec or 0.1465 arcsec/pixel. The 68.7 mm diagonal dimension across the CCD mentioned in item 12 implies that the camera field radius must be at least 5.20 degrees to support the spectral-imaging requirement.

The fact that in effect, VPH gratings are used in Littrow as mentioned in item 5, means that the expected anamorphic factors at the camera will depend only on the angle of incidence at the grating (Q/2) and the maximum field angle at the camera *in the dispersion direction.* Item 5 limits the incidence angle to 45.0 degrees while the maximum dispersion angle at the camera is +/- 4.66 degrees at the red/blue extremes, respectively. Thus one finds that the most extreme anamorphic factors expected will be cos(45.0+4.66)/cos(45.0)=0.915 at the red end and cos(45.0-4.66)/cos(45.0)=1.078 at the blue end. These anamorphic factors are modest compared with traditional (surface-relief) reflection gratings which are typically used far out of Littrow such that the range of anamorphic factors is much larger. The modest anamorphic factors derived for VPH gratings aid greatly in designing the camera because its entrance aperture will not have to be so large to accept the off-axis pupils. Another way of saying the same thing is that for a given aperture size, significantly less vignetting is expected with VPH gratings as compared with surface-relief reflection gratings.

The maximum spectral resolution of 8000 mentioned in item 7 implies a reciprocal dispersion of 13.89 Angstroms/mm (at 0.50 microns with 3-pixel sampling). This would require a grating with about 1721 lines/mm if used in 1st order. However if the slit is opened to a 0.50-arcsec width and the PSF degrades the image by 0.18 arcsec as mentioned in item 4, then the effective sampling will be about 4.64 pixels such that a reciprocal dispersion of 8.975 Angstroms/mm would be needed. This would require a grating with about 2376 lines/mm to achieve the desired resolution of 8000 if used in 1st order. Fine spacings such as these are practical with VPH gratings. If the VPH fringes are normal to the grating surface (as usually chosen) the required grating angles would be the same as for plane surface-relief reflection gratings, namely 25.52 degrees and 36.44 degrees respectively. The anamorphic factors would be quite modest as described in the previous paragraph. Thus a resolution of 8000 seems realizable.

3.2 Workable Image Quality Targets for Collimator and Camera

In order to convert the PSF blurring limit mentioned in item 4 into workable image quality targets for the collimator and camera, we began by assuming that a 0.50 arcsec image will be broadened 0.18 arcsec due to the collimator blur, the camera blur and to the Nyquist limit of the 15 μm pixels. Assuming that these effects add in quadrature and converting into pixel units, one finds:

$$3.413^2 + (\text{collimator blur})^2 + (\text{camera blur})^2 + (2.0)^2 = (3.413 + 1.229)^2. \qquad (4)$$

Based on previous experience, most of the error budget was reserved for the collimator, because of the difficulty in attaining super-sharp images over the full passband. Assuming that *linearly* the collimator blur at the camera imaging scale will be *twice as big* as the camera blur and using equation 4, one has:

$$5.0 \times (\text{camera blur})^2 = (3.413 + 1.229)^2 - (3.413)^2 - (2.0)^2, \quad (5)$$

which works out to a very small camera blur of 1.086 pixels or 16.3 μm.

A workable definition of *camera blur* is the rms image diameter averaged over all wavelengths and field angles that the camera must service. That number will have a dispersion about the mean and this was incorporated by setting a target rms image diameter of 13.0 +/- 3.3 μm or better , and insisting that the worst-case image(s) not exceed the mean + 2 units of variation, or 19.6 μm. The image evaluation must be done over the full 320-850 nm passband without refocus as mentioned in item 6. In addition to this target for image blur, a separate target for lateral color was established, somewhat arbitrarily, at less than 75% of the rms image diameter, or 9.8 μm.

As in equation 5, the image quality target for the collimator is to produce images whose averaged rms diameter do not exceed twice the camera blur, after demagnification by the 3.1816 scale factor. At the collimator's imaging scale, this becomes 82.7 +/- 21.0 μm with the worst-case image(s) less than 124.7 μm. This is at the same imaging scale as the telescope itself (325.8 μm/arcsec) so the collimator targets are 0.25 +/- 0.06 arcsec and 0.38 arcsec, worst-case. These targets seem gross compared with the goal of not degrading a 0.50-arcsec image by more than 0.18 arcsec, but *they do work out*, assuming the aberrations are random such that they can be added in quadrature. The lateral color target for the camera was 9.8 μm rms which is about 0.10 arcsec. Since lateral color adds linearly to the smear in imaging mode, and since the collimator's lateral color *might add linearly* to that of the camera, the target adopted for the collimator's lateral color was *as small as possible*. In practice that proved to be about 0.04 arcsec, as will be seen in the next section.

3.3 Collimator optical design and performance

The collimator design began as a {singlet} {singlet}{singlet} {triplet} element configuration with a focal length of 1200.5 mm (47.25 inches) . The materials were limited to fused silica, CaF2, NaCl with Cargille Laser Liquid Type 5610 of n(D)= 1.4750 as the coupling fluid, in keeping with the bandpass requirements mentioned in item 2. Furthermore, all surfaces were constrained to be spherical. The first singlet was placed close to the telescope focal surface to help move the exit pupil close to the last element as stipulated in item 10. The triplet was introduced to provide most of the power and chromatic correction, as well as a buried location for an NaCl element, to protect it from moisture. The two singlets provide extra degrees of freedom by migrating as needed. The main difficulties in this configuration are the potential for exit pupil aberrations, and the difficulty in achieving adequate chromatic correction using the limited selection of UV transmitting materials.

The initial design was optimized by Epps using his proprietary code OARSA. During this process it was possible to discard one of the singlets and to retain all spherical surfaces, but it proved impossible to substitute a more durable material for the NaCl. The process for growing large NaCl crystals and the technology for making them into high quality optical elements is well developed, and no problem is anticipated with its use in this design. The optimized design is shown in Figure 5 as a suggested preconstruction collimator. The telescope and lens prescriptions are listed in the appendix, as are the Schott-formula dispersion coefficients used for the materials. The collimator designs shows an rms image diameter of 0.19 +/- 0.05 arcsec averaged over all field angles and wavelengths within the 320-850 nm passband (without refocus), with 0.04 arcsec of maximum rms lateral color. There is a 0.06% maximum residual 3rd order pincushion distortion which is "none" for all intents and purposes. Lateral color analysis shows that this collimator has virtually no lateral color of any consequence. It is clear that the imaging performance is better than target values such that one could reasonably expect this collimator to exceed the image quality goal stipulated in item 4 by a comfortable margin. The polychromatic image of the telescope pupil formed by the collimator measures 75.06 mm for an "on-axis" star, and wanders by only 0.7 mm for a star at the full 3.6' field radius, with minimal distortion. Thus the pupil is stable to abut 0.9%, which is better than we require.

3.4 Camera optical design and performance

The camera design began as a {doublet} {sextet} {doublet} {singlet} configuration, where the last singlet also serves as the vacuum dewar window. The focal length was 377.2 mm (14.85 inches) with an entrance pupil distance of 88.9 mm, following the guidline in item 10. To avoid vignetting with an anamorphic factor of 1.1, the entrance diameter is 101.6 mm (4 inches). This anamorphic factor is somewhat larger than the maximum achieved at the edges of the field angle in the

dispersion direction when the included angle Q reaches 90 degrees. The resulting camera has a modest f/3.71 geometric focal ratio.

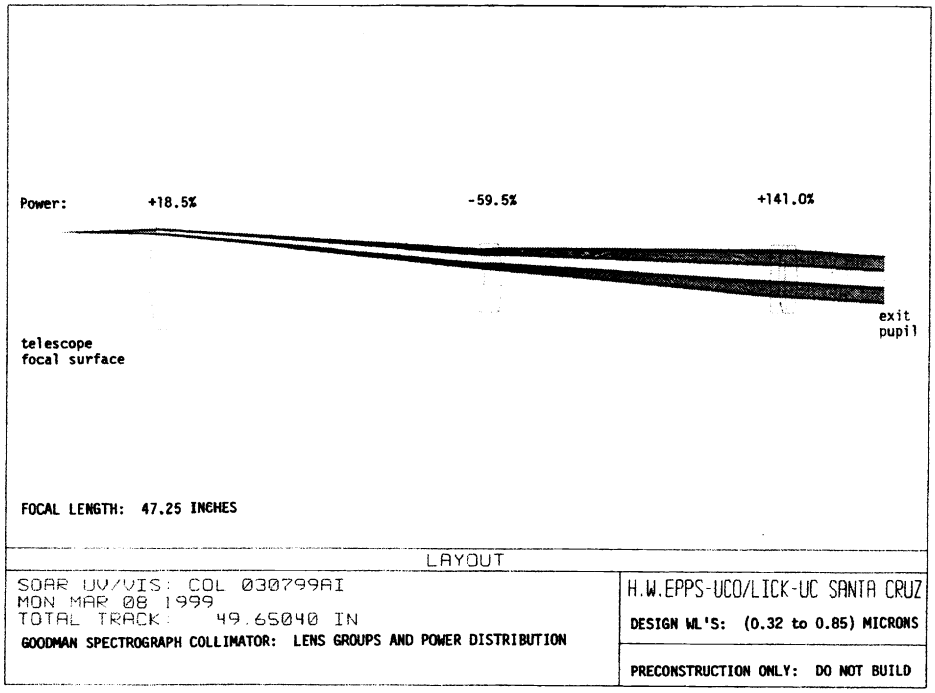

Figure 5: Scaled drawing of suggested pre-construction collimator. The materials and prescription data are listed in the appendix.

The starting optical configuration showed promising image quality, but unacceptable lateral color. During the design optimization, it became apparent that reducing the sextet to a symmetric quintet, and eventually to a triplet improved the lateral color while reducing the number of elements and coupling boundaries in nice compliance with item 14 in the design goals. Figure 6 shows the suggested preconstruction camera resulting from the full optimization. It has a length of 495.0 mm, and together with the collimator gives a total system length of 1624 mm from the telescope focal surface to the camera focal plane, 17 mm less than the target in item 9. In spectroscopic mode, the camera shows an rms image diameter of 13.6 +/- 3.3 μm averaged over all field angles and wavelengths within the 320 to 850 nm passband (without refocus), with 7.5 μm of maximum rms lateral color. There is a 0.06% maximum residual 3rd order barrel distortion. Analysis of monochromatic images at a range of field angles and extending *beyond* the design spectral range show performance comparable to the target values for *imaging mode* so that one might reasonably expect this camera to exceed the image quality goal stipulated in item 4, again by a comfortable margin.

3.5 System Performance in Imaging Mode

Figure 7 shows polychromatic imaging performance over the full 320 to 850 nm passband for the *integrated system* in imaging mode. At the field edge, 50% of the energy *over the entire passband* is contained within a 1.69 pixel diameter (0.248 arcsec). Adding in quadrature (still in pixel units) one has:

$$(3.413)^2 + (1.69)^2 + (2.0)^2 = (4.30)^2, \qquad (6)$$

equivalent to a FWHM image diameter of 0.630 arcsecs. This represents 0.13 arcsec degradation of 0.5 arcsec seeing, considerably better than the 0.18 specified in item 4. Even if the image diameter definition in item 4 had been a 70% energy diameter instead of FWHM but the rest of the stipulation had been the same, the degradation is only 0.176 arcsec, *just a bit*

less than the allowed 0.18-arcsec limit! Impressive performance considering that the star image would only have been 0.38 arcsec FWHM, as tall a tale as ever told about the seeing at any site.

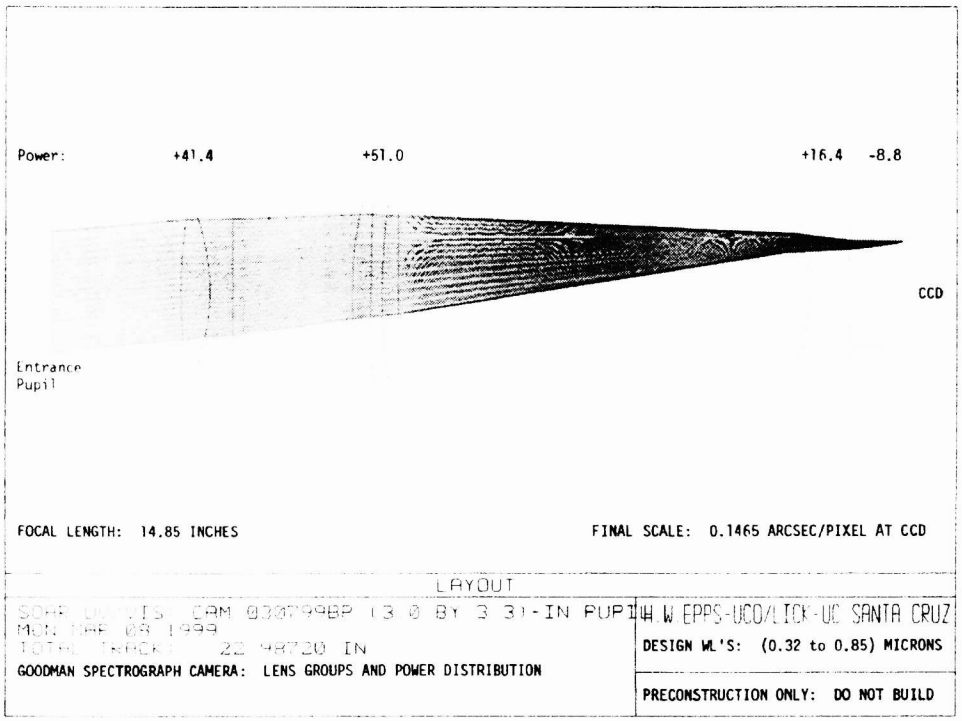

Figure 6: Scaled drawing of suggested pre-construction camera. The materials and prescription data are listed in the appendix.

3.6 Conclusions

It has proved possible to design an attractive all-spherical camera and collimator for the Goodman Spectrograph that make use of VPH gratings. The optics are designed to operate over the full passband without refocus, and meet or exceed the image quality goals established for the Goodman Spectrograph. They use only materials with essentially 100% internal transmission in the UV and there are no mirrors in the system. When combined with highly efficient and tunable VPH gratings, the result should be an imaging spectrograph with extraordinarily high photon efficiency and tight image concentration capable of taking advantage of the image quality delivered by the SOAR telescope.

4. REFERENCES

1. V. L. Krabbendam, G. P. Ruthven, M. E. Furber, J. T. Stein, Active optical system design for the 4.2-m SOAR telescope, *Proceedings SPIE* **This Volume**, 2000.
2. Gerald Cecil, "Summary of SOAR partner science", *http://www.physics.unc.edu/soar/SOAR/science.pdf*, 2000.
3. Samuel C. Barden, James A. Arns, and Willis S. Colburn, "Volume-phase holographic gratings and their potential for astronomical applications", *Proceedings SPIE* **3355**, pp. 866-876, 1998.
4. Thomas K. Gaylord and M. G. Moharam, "Analysis and applications of optical diffraction by gratings", *Proceedings IEEE* **73,** pp 894-937, 1985.
5. Richard D. Rallison, *private communication,* 1999.
6. H. Kolgelnik, "Coupled wave theory for thick hologram gratings", *Bell Syst. Tech. J.* **48**, pp. 2909-2947, 1969.
7. M. G. Moharam, T. K. Gaylord, and R. Magnusson, "Criteria for Bragg regime diffraction by phase gratings", *Opt. Commun.* **32**, pp 14-18, 1980.
8. Richard D. Rallison, "Phase materials for HOE applications", *http://www.xmission.com/~ralcon/phasemat.html*, 2000.
9. Harland W. Epps, "Development of large high-performance lenses for astronomical spectrographs", *Proceedings SPIE* **3355**, pp.111-128, 1998.

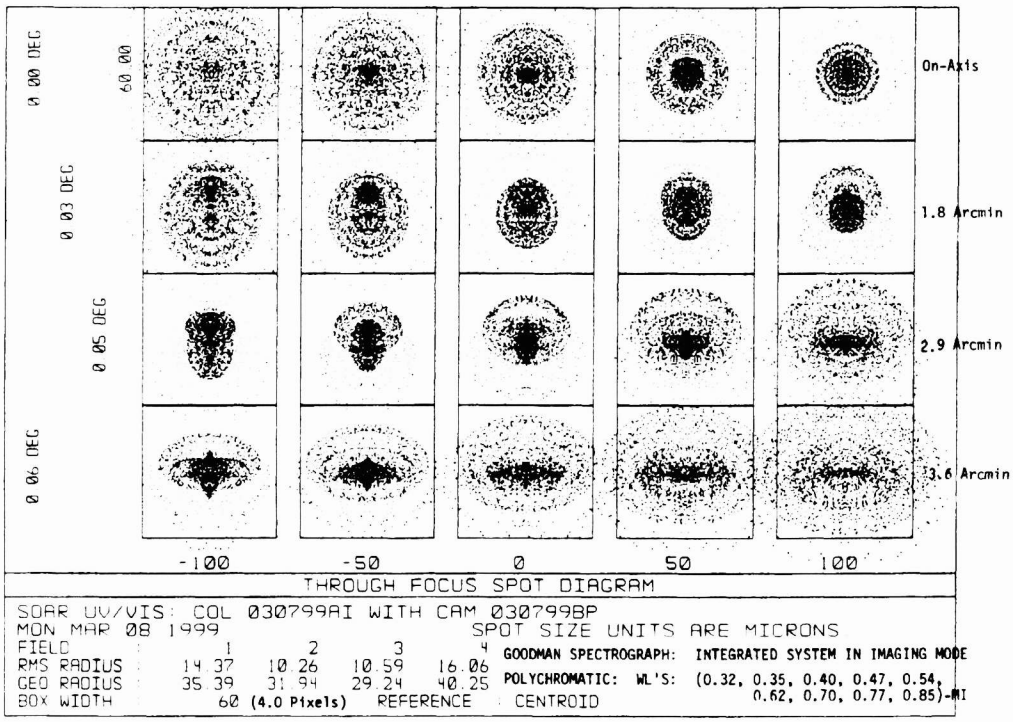

Figure 6: Through focus polychromatic spot diagrams for integrated system in imaging mode.

5. APPENDIX

For a description of the conventions used in this appendix, see Epps[9].

Schott Formula Dispersion Coefficients for Optical Materials

CaF_2	A0 = 2.0388472 x 10^{0}	A1 = -3.2320997 x 10^{-3}	A2 = 6.1568960 x 10^{-3}
	A3 = 5.6612714 x 10^{-5}	A4 = -4.0951444 x 10^{-9}	A5 = 2.2406560 x 10^{-8}
Fused Silica	A0 = 2.1045254 x 10^{0}	A1 = -9.5251763 x 10^{-3}	A2 = 8.5795589 x 10^{-3}
	A3 = 1.2770234 x 10^{-4}	A4 = -2.2841020 x 10^{-6}	A5 = 1.2397250 x 10^{-7}
NaCl	A0 = 2.3300477 x 10^{0}	A1 = -9.4085558x 10^{-4}	A2 = 1.8063105 x 10^{-2}
	A3 = 3.5052613 x 10^{-4}	A4 = 2.6039433 x 10^{-6}	A5 = 3.5339426 x 10^{-7}
LL-4750	A0 = 2.1271487 x 10^{0}	A1 = -2.7177429 x 10^{-3}	A2 = 1.3819986 x 10^{-2}
	A3 = 1.7327102 x 10^{-3}	A4 = -2.4144212 x 10^{-4}	A5 = 1.4179229 x 10^{-5}

SOAR 4.2 M F/16.0 with 47.25 inch pre-construction collimator

Identification	Clear Diameter	material	sag	curvature	thickness	A2
Stop	165.354	AIR	0.000	0.0 x 10^{0}		
Primary	166.170	AIR	-6.497	-1.8824215 x 10^{-3}	-2.2952756 x 10^{2}	-10.03174

Secondary	23.134	AIR	-0.832	$-1.2464108 \times 10^{-2}$	3.5945300×10^{2}	-1.528320
Focal Surface	5.623	AIR	-0.105	$-2.6486558 \times 10^{-2}$	5.8303	
Element 1	6.113	SILICA	0.363	7.6567446×10^{-2}	1.1999998	
	6.028	AIR	0.031	6.7495769×10^{-3}	1.8783578×10^{1}	
Element 2	3.771	SILICA	-0.260	$-1.4369614 \times 10^{-1}$	1.0000003	
	3.873	AIR	-0.148	$-7.8394189 \times 10^{-2}$	1.6080526×10^{1}	
Element 3	3.781	SILICA	-0.026	1.4365821×10^{-2}	0.49999881	
	3.768	LL-4750	0.154	8.5969166×10^{-2}	2.9999929×10^{-3}	
Element 4	3.768	NaCl	0.154	8.5969166×10^{-2}	0.29999929	
	3.756	LL-4750	0.176	9.8666158×10^{-2}	2.9999929×10^{-3}	
Element 5	3.756	CaF_2	0.176	9.8666158×10^{-2}	0.75000086	
	3.750	AIR	-0.110	$-6.2075429 \times 10^{-2}$	5.2013180	

14.85 inch F/3.71 (geometric) pre-construction camera

Identification	Clear Diameter	material	sag	curvature	thickness
	3.300	AIR	0.000		3.50000
Element 1	3.997	CaF_2	0.158	7.8597295×10^{-2}	0.80000
	4.008	LL-4750	-0.353	$-1.7067361 \times 10^{-1}$	2.9999970×10^{-3}
Element 2	4.008	SILICA	-0.353	$-1.7058626 \times 10^{-1}$	0.59999999
	4.050	AIR	0.009	4.5653716×10^{-3}	3.2248853
Element 3	4.299	CaF_2	0.222	9.5191574×10^{-2}	0.50000000
	4.275	LL-4750	0.038	1.6824751×10^{-2}	2.9999970×10^{-3}
Element 4	4.275	NaCl	0.038	1.6825600×10^{-2}	0.3000000
	4.245	LL-4750	0.134	5.9241145×10^{-2}	2.9999970×10^{-3}
Element 5	4.245	CaF_2	0.134	5.9251675×10^{-2}	0.42500001
	4.227	AIR	-0.011	$-4.9118744 \times 10^{-3}$	10.309456
Element 6	3.196	CaF_2	0.258	1.9712208×10^{-1}	0.7000000
	3.127	LL-4750	-0.192	$-1.5456818 \times 10^{-1}$	2.9999970×10^{-3}
Element 7	3.126	SILICA	-0.192	$-1.5449654 \times 10^{-1}$	0.99999999
	2.803	AIR	0.098	$-9.9604193 \times 10^{-2}$	0.35000001
Element 8	2.776	SILICA	-0.149	$-1.5253892 \times 10^{-1}$	0.85000000
	2.749	AIR	0.077	8.1763718×10^{-2}	0.41073302